NRL Memorandum Report 4380

Laser-Initiated, Reduced Density Channels for Transporting Charged Particle Beams

M. Raleigh, J.R. Greig, R.E. Pechacek, and E. Laikin

Experimental Plasma Physics Branch
Plasma Physics Division

February 13, 1981

Research supported by the Office of Naval Research and by Defense Advanced Research Projects Agency (DoD) ARPA Order No. 3718, monitored by the Naval Surface Weapons Center under Contract N60921-80-WR-W0189

NAVAL RESEARCH LABORATORY
Washington, D.C.

(14) NRL-MR-4380

(9) Memorandum rept.

SECURITY CLASSIFICATION OF THIS PAGE (When Data Entered)

REPORT DOCUMENTATION PAGE		READ INSTRUCTIONS BEFORE COMPLETING FORM
1. REPORT NUMBER NRL Memorandum Report 4380	2. GOVT ACCESSION NO. AD-A095	3. RECIPIENT'S CATALOG NUMBER 725
4. TITLE (and Subtitle) (6) LASER-INITIATED, REDUCED DENSITY CHANNELS FOR TRANSPORTING CHARGED PARTICLE BEAMS		5. TYPE OF REPORT & PERIOD COVERED Interim report on a continuing problem
		6. PERFORMING ORG. REPORT NUMBER
7. AUTHOR(s) (10) M. Raleigh, J.R. Greig, R.E. Pechacek and E. Laikin		8. CONTRACT OR GRANT NUMBER(s) (11) 13 Feb 81
9. PERFORMING ORGANIZATION NAME AND ADDRESS Naval Research Laboratory Washington, D.C. 20375 (12) 34		10. PROGRAM ELEMENT, PROJECT, TASK AREA & WORK UNIT NUMBERS 61153N; R011-09-41; 67-0871-0-0 and 61101E; 0; OR40AA
11. CONTROLLING OFFICE NAME AND ADDRESS Office of Naval Research, Arlington, VA 22217 Defense Advanced Research Projects Agency Arlington, VA 22209 ATTN: Program Management		12. REPORT DATE February 13, 1981
		13. NUMBER OF PAGES 32
14. MONITORING AGENCY NAME & ADDRESS (if different from Controlling Office) Naval Surface Weapons Center White Oak, MD 20910 ATTN: Code R401		15. SECURITY CLASS. (of this report) UNCLASSIFIED
		15a. DECLASSIFICATION/DOWNGRADING SCHEDULE

16. DISTRIBUTION STATEMENT (of this Report)

(15) ARPA Order-3718 (16) RO1109

Approved for public release, distribution unlimited.

(17) RO110941

17. DISTRIBUTION STATEMENT (of the abstract entered in Block 20, if different from Report)

18. SUPPLEMENTARY NOTES

Research supported by the Office of Naval Research and by the Defense Advanced Research Projects Agency (DoD) ARPA Order No. 3718, monitored by the Naval Surface Weapons Center under Contract N60921-80-WR-W0189.

19. KEY WORDS (Continue on reverse side if necessary and identify by block number)

Charged Particle Beam
Transport
Reduced Density Channel

20. ABSTRACT (Continue on reverse side if necessary and identify by block number)

A charged particle beam driven inertial confinement fusion reactor will require reduced density, current carrying channels through the gas blanket to transport the beams from the diodes to the target. We have created suitable reduced density channels in air at atmospheric pressure by guiding an electric discharge with laser-induced, aerosol-initiated air-breakdown. The resulting channel which is no longer current carrying stabilizes, $\simeq$30 μs after the electric discharge, at a radius of ~1 cm, a temperature of ~5000°K, a gas density of $\simeq 10^{18}$ cm^{-3} and an electron density of $\simeq 10^{14}$ cm^{-3}.

(Continued)

DD FORM 1473, 1 JAN 73 EDITION OF 1 NOV 65 IS OBSOLETE
S/N 0102-014-6601

i SECURITY CLASSIFICATION OF THIS PAGE (When Data Entered)

251950

20. ABSTRACT (CONTINUED) about 100 microsec

After ~100 μs the channel both becomes turbulent and expands further. We provide estimates of the diminishing temperature and increasing density during this later phase.

The desired reduced-density, current carrying channel can be produced by a second fast rising, high current discharge on the described channel, after the stable reduced density conditions have been achieved.

CONTENTS

LASER-INITIATED, REDUCED DENSITY CHANNELS FOR TRANSPORTING CHARGED PARTICLE BEAMS

I. INTRODUCTION

Recent charged particle beam fusion reactor designs propose using multiple diodes, protected from the target by a high density gas blanket, with reduced-density, laser-initiated, current carrying plasma channels to transport and combine the beams.[1] Multiple diodes are necessary to reach the required beam power levels. Low density, electrically conductive, and current carrying channels are necessary to minimize beam particle scattering, neutralize the beam electric and magnetic fields, and provide magnetic guide fields.[2,3] Beam transport experiments to date have used wire-initiated electric discharges and wall stabilized z-pinches[2,3,4] to create such channels but neither approach is suitable for a repetitively pulsed fusion reactor.

Previous experiments have shown the ability of residual levels of ionization in air, resulting from CO_2 laser-induced, aerosol-initiated air-breakdowns, to guide long electric discharges at low applied field strengths and at large angles to the field direction[5]. The production, by this same means, of V-shaped electric discharges demonstrates the feasibility of producing multiple channels intersecting at the target location[6].

In this experiment[7] we have used a Nd:glass laser, focused into aerosol doped air, to produce long strings of laser breakdown beads. The disturbance caused by these beads was used to guide a high voltage electric discharge. Following this discharge there evolved a straight, radially uniform, low density, electrically conducting channel. We estimated conditions in this channel from electrical circuit measurements and from the channel dynamics as seen in open shutter and Schlieren photographs. We also

Manuscript submitted October 14, 1980.

observed the later disruption of the channel through turbulence and we used a simple model to estimate the resulting conditions.

Because the high voltage discharge was of short duration ($\sim 6\ \mu$sec) compared to the hydrodynamic expansion time of the channel ($\sim 30\ \mu$sec), there was no current flowing in the channel by the time it had evolved to the low density, atmospheric pressure state. However with the use of a suitable high voltage switch, a second current pulse can be created in the low density channel to provide the magnetic guide field required for transporting particle beams.[8] The second discharge must be fast enough so that no hydrodynamic or magnetic instabilities can develop in the channel before the desired current has been achieved. Rise-times of 5 to 10 μsec are adequate.

II. APPARATUS AND EXPERIMENTAL PROCEDURE

The apparatus used for this experiment in shown in Figure 1. A Q-switched 60 J Nd:glass laser was used to produce strings of laser breakdown beads.[9] As used the laser had a peak power of $\sim 1.5\times10^9$ W, a pulse width of $\sim$40 ns (FWHM) and a divergence angle of $\sim 4\times10^{-4}$ radians. The laser was focused with a $\sim$5 m focal length lens resulting in a minimum focal spot $\sim$.2 cm in radius with a peak on axis intensity of $\sim 1.6\times10^{10}$ W/cm^2. The laser intensity never reached the clean air breakdown threshold of $\sim 3\times10^{11}$ W/cm^2, however, the breakdown threshold was lowered by the presence of aerosols[10]. The aerosols were produced by burning black gunpowder. A variac controlled, hot nichrome wire ignited the powder in a small tray. A desk fan dispersed the aerosols throughout the enclosure. In a few minutes a nearly uniform dispersion was achieved. The enclosure was $\sim 3\times3\times5$ m and $\sim$2.5 g. of gunpowder was burned to yield an aerosol loading of $\sim .1\ \mu$ g/cm^3. When the air in the enclosure was not stirred, aerosols capable of causing profuse breakdowns persisted for $\sim$1 hr.

The high voltage pulse to drive the electric discharge was provided by a small Marx generator ($V \sim 360$ kV, $C \sim .015\ \mu$F, $R_{int} \sim 4.5\ \Omega$, $L_{int} \sim 6\ \mu$H) which was normally charged to 250 kV in these experiments. The internal connections of this generator are shown in Figure 2. We found that when

the high voltage pulse was applied between ~10 and ~ 100 μs after the laser had fired, reliable guiding occurred. A delay time of ~ 30 μs was adopted for the channels used in this experiment.

The channel was photographed from the side and above with open shutter cameras. Streak photographs were taken with a STL model 1-D image converter camera. Schlieren photographs were taken using a Korad model K-1 pulsed ruby laser and the optical system shown in Figure 3. Time integrated spectra were taken of the channel using a Spex 3/4 m spectrograph. The electric discharge current was monitored with a Rogowski coil and the Marx output voltage with a capacitative voltage divider. The timing electronics to trigger the Nd:glass laser, the Marx generator, the ruby laser, and the image converter camera were located in a copper screened Faraday enclosure and the signal leads shielded in copper tubing. The diagnostic signals were brought to the Faraday enclosure in copper tubing and recorded on oscilloscopes.

The channel was also formed in atmospheric pressure Argon. A sealed nonconducting box was used to hold the Argon which had windows to admit the Nd:glass laser and the ruby laser Schlieren beam. Aerosols from black powder were again used.

III. RESULTS AND DISCUSSION

The breakdown beads created by the interaction of the Nd:glass laser with the aerosol doped air extended from ~4.5 m from the lens, through focus, to a point ~7 m from the lens to give a total length of the string of breakdown beads of ~2.5 m. The beads were closely spaced and confined to a channel ~.2 cm in radius (Fig. 4). Calorimeter measurements showed ~15 J/m were absorbed from the laser beam by the string of breakdown beads.

The electric discharge was guided, provided the laser breakdown beads were closely spaced from the high voltage to the ground electrode. Discharges of up to 2 m long have been produced using the ~2.5 m string of laser breakdown beads. If gaps of more than a few cm existed in the string of breakdowns, guidance became sporadic and if guidance did occur the gaps were bridged by loops in the discharge (Fig. 5). Otherwise the luminous discharge, as seen in the open shutter photographs (Fig 4),

did not deviate from the envelope containing the laser breakdowns. The discharge appeared to zig-zag between the breakdown bead locations and to be more diffuse when in the vicinity of a bead. Streak photographs (Fig. 6) indicated that the laser breakdown beads were non-luminous by the time of application of the discharge voltage. Granularity nevertheless remained evident in the luminosity of the electric discharge.

The Schlieren photographs show that the laser disturbances coalesced in time to form a quasicontinuous region ~.25 cm in radius. The laser energy deposited in this region was thus ~ 1 J/cm^3. Greig et al. found that the deposition of similar amounts of energy from a CO_2 laser resulted in the guidance of electric discharges nearly perpendicular to the direction of the electric field and at velocities characteristic of the return stroke of a long spark.[5] Our closure velocity of ~10^9 cm/s was in reasonable agreement with their results for a similar applied voltage. Our time range of ~10 to ~100 μs for good guidance was also in agreement with their work. It is therefore reasonable to presume that guidance was caused by similar mechanisms, wherein an electron density between 10^8 and 10^{12} cm^{-3} persisted, following the laser breakdown, and was sustained by collisional detachment from O_2^- ions. The persistence of this enhanced conducitivity permitted the propagation of a potential wave carrying substantially the entire high voltage. The ability of our discharge to bridge small gaps in the breakdown beads supports this hypothesis (Fig. 5). Our observations also indicate that the residual electron density varied spacially, being highest where the center of a breakdown bead had been located (Fig. 4).

The expansion of the channel, following the electric discharge, was observed by Schlieren photography (Fig. 7). The average channel radius was estimated from these photographs and plotted as a function of time (Fig. 8). The discharge first created an irregular ohmicly heated channel ~.25 cm in radius having the approximate outline of the original aerosol disturbances. This expanded to a ~1 cm radius channel with irregular boundaries but a uniform core. (Also evident in the Schlieren photographs are expanding shocks due to both the initial laser breakdowns and the ohmic heating.) Between ~30 and ~100 μs the channel remained at approximately the same radius and was therefore in pressure equilibrium with the surrounding atmosphere. Thereafter the channel both became turbulent and

expanded in radius again. A superimposed white light and Schlieren image, taken 12 μs after the discharge voltage was applied, suggests that, as the channel expanded to pressure equilibrium, the crookedness of the initial discharge determined the roughness of the edge of the expanded channel (Fig. 10). Schlieren photographs taken at both electrodes and in the middle of the channel showed it to be uniform from end to end (Fig. 11). Time integrated spectra were taken of the channel and showed no contamination that could be attributed to the use of aerosols (Fig. 12).

The initial expansion of the discharge heated channel to a stable ~ 1 cm radius appeared to take place without convective mixing between the hot channel gas and the outside air. Furthermore, diffusion will not be significant on the time scale of this expansion. Thus this channel contained only the matter present prior to expansion and had a density of $\sim 1/20$ atmospheric corresponding to the $\sim 20:1$ volume change which took place. The temperature of the channel, for times of ~ 30 to $\sim 100\ \mu s$, may be estimated by assuming pressure balance with the outside atmosphere. The establishment of pressure balance is consistent with sound velocities inside and outside the channel. The molecules in the channel were both partially dissociated and hotter to equal the pressure of the higher density outside air Letting n_f represent the post expansion molecular density, T_f the temperature and α the fractional dissociation we may write

$$T_f = \frac{n_0}{(1+\alpha)n_f} T_0 \tag{1}$$

The ratio of molecular densities is given by the volume change as 20:1. As the fractional dissociation, α, is a function of the final temperature, self consistent values of T_f and α must be sought. The quantity $(1+\alpha)$, as a function of temperature, may be determined from the tables of Burhorn and Wienecke[11] which give the equilibrium composition of air at elevated temperatures (Fig. 13). Using this Figure, the temperature and fractional dissociation are found to be $T \sim 5000\,°K, \alpha \sim .2$. Burhorn and Wienecke also tabulate specific enthalpy as a function of temperature from which energy per molecule (ϵ) as a function of temperature at 1 atmosphere has been plotted (Fig. 14.). Using this graph we find $\epsilon_f \sim 2.7$ ev./mol.

Assuming the channel expanded adiabatically, we may find the pre-expansion conditions. We may write

$$P_i = \left(\frac{V_f}{V_i} \right)^{\gamma} P_f \tag{2}$$

where P and V are pressure and volume, γ is the ratio of specific heats, and subscripts f and i relate to the final and initial states respectively. Zeldovich and Raizer[12] give the effective γ for standard and reduced density air as a function of temperature (Fig. 15). The value $\gamma \sim 1.2$ is appropriate for the temperature range in this situation and yields an initial pressure of 36 atmospheres. Zeldovich and Raizer also give temperature and energy for standard and reduced density air as a function of pressure (Fig. 16). From this figure we determine the initial temperature and energy to be $T_i \sim 7000\,°K$ and $\epsilon_i \sim 4.6$ ev./mol. This corresponds to an energy deposition of ~ 3.5 J/cm of channel length.

The electrical energy deposited in the channel may be determined from the electrical characteristics of the discharge. The voltage and current signals closely approximate the response of an underdamped RLC circuit of constant R (Fig. 17). It is therefore possible to determine the circuit inductance and resistance from measurements of the period, T, and the damping constant δ

$$L = \frac{1}{C} \left(4 \frac{\pi^2}{T^2} - \delta^2 \right)^{-1} \tag{3}$$

$$R = 2L\delta. \tag{4}$$

Measurements were made on both the shorted Marx generator and the Marx generator driving a $.5m$ channel. Thus it was possible to determine both the internal Marx resistance and the channel resistance. The total stored energy ($CV^2/2 = 625$ J.) was divided between the internal and channel resistance giving an energy deposited in the channel of ~ 3.5 J/cm, which is in good agreement with the value deduced from the channel dynamics and supports the adiabatic assumption.

After $\sim 150\ \mu$sec the channel became turbulent and expanded again. With no external sources of energy, expansion was only possible because additional outside air was being entrained and mixed into the channel. The hot gas in the channel possessed energy of vibration and dissociation in addition to its

kinetic energy. When mixing began, and cooled the channel, this extra energy was released, which provided the impetus for continued expansion and mixing. The process happened continuously and in such a way as to maintain atmospheric pressure but was also rather non-uniform. However, we have adopted the simple model of alternating small steps of mixing and adiabatic expansion assuming uniform mixing in order to estimate the temperature and density during this process. Starting from the stable, hot channel conditions (r_o, n_o, T_o) , we take a small increment in radius and presume the cold outside air within this layer mixes thoroughly with the channel. Within this new radius the molecular density, n_i, and energy, ϵ_i, are obtained by conserving particles and energy.

$$n_i = \frac{n_o r_o^2}{r_i^2} + 2.55 \times 10^{19} \frac{(r_i^2 - r_o^2)}{r_i^2} \qquad \text{cm}^{-3} \tag{5}$$

$$\epsilon = \frac{1.65 \times 10^{18} (r_i^2 - r_o^2)}{n_i r_i^2} + \frac{\epsilon_o n_o r_o^2}{n_i r_i^2} \qquad \text{ev.} \tag{6}$$

From this energy, using Figure 14, we find a new temperature, T_i. The dissociation, α, at this temperature is found from Figure 13 allowing us to evaluate the hypothetical pressure

$$P_i = \frac{(1+\alpha) n_i T_i}{7.65 \times 10^{21}} \qquad atm. \tag{7}$$

We now allow the adiabatic expansion, without further mixing, to bring the channel back to atmospheric pressure. The final radius is then

$$r_f = r_i P_i^{\frac{1}{2\gamma}} \qquad \text{cm} \tag{8}$$

where the appropriate γ for temperatures near T_i is found using Figure 15. Because no new particles have been introduced we have

$$n_f = \frac{n_i r_i^2}{r_f^2} \qquad \text{cm}^{-3} \tag{9}$$

knowing atmospheric pressure has been re-established, we find

$$T_i = \frac{7.65 \times 10^{21}}{(1+\alpha) n_f} \qquad {}^\circ K \tag{10}$$

where it is generally sufficiently accurate to use the value of α at T_i. Lastly we may find the final energy, ϵ_f by again using Figure 14.

These final conditions, (n_f, r_f, T_f) are now taken as new initial conditions and the whole process repeated. In this way temperature and density as a function of channel radius are determined and by reference to Figure 8 they may be determined as functions of time. These results are shown in Figure 18.

Channels formed in Argon (Fig. 9) showed the same turbulence, at late times, as those in air. While the total internal energy of the Argon will not include rotational, vibrational or dissociation contributions, there will be excess energy due to atomic excitation (particularly metastable states).

IV. CONCLUSIONS

We have guided a fast high voltage discharge with laser-induced air-breakdown to produce a straight, radially uniform, reduced density channel. The channel is stable for $\sim 70\ \mu s$, thereafter becoming turbulent and expanding. During the stable phase the channel temperature is $\sim 5000\,°K$.

The elevated temperature results in an electron density[13] of $\sim 10^{14}\ cm^{-3}$. This results in a electrical conductivity of $\sim$ 30 $(ohm-m)^{-1}$ determined by electron-neutral collisions. It is therefore possible for a second lower voltage but high current discharge to be conducted through the channel. Such a second discharge, provided it has a rise time of $\lesssim 5\ \mu s$, will produce magnetic guide fields before the channel expands further or kinks. Methods of impressing this second discharge are presently under test at NRL.

The size ($r \sim 1$ cm) and density ($\rho \sim \rho_o/20$) of the stable channel are determined by the electrical energy input, the background gas density, and possibly the diameter of the laser beam. The combinations of channel radius and density which are achievable will be investigated in future experiments.

Our channel is presently limited to $\sim$ 2 m in length by the properties of the Nd:glass laser. Air breakdowns of up to $\sim$60 m in length using Nd:glass lasers have been reported however,[14] and it may

be possible to guide an electric discharge over such distances. Our laser will be upgraded in the near future to permit investigation of such long breakdowns.

We have used aerosols to initiate the air breakdown. However, any absorbtion mechanism which results in a residual electron density of $\lesssim 10^9$ cm^{-3} along the laser path could be used to initiate the channel production process. Thus, while our specific methods may not be directly applicable to any given reactor scenario, they nevertheless allow us to investigate the properties of the channels formed by laser guided discharges and it appears channels suitable for a charged particle beam transport may be formed by this means.

V. ACKNOWLEDGEMENTS

We gratefully acknowledge the helpful discussions we have had with, and comments we have received from Drs. A.W. Ali, R.F. Fernsler, R.B. Fiorito, M. Lampe, A.E. Robson and I.M. Vitkovitsky. We also acknowledge the assistance of Laura Allen in performing this experiment.

VI. REFERENCES

1. G. Yonas, Sci Amer. *239* (5), 50-61 (1978)

2. P.A. Miller, R.I. Butler, M. Cowan, J.R. Freeman, J.W. Poukey, T.P. Wright, and G. Yonas, Phys. Rev. Lett *39*, 92-94 (1977)

3. J. Benford, J. Appl. Phys. *48*, 2320-2323 (1977)

4. F.L. Sandel, F.C. Young, S.J. Stephanakis, F.W. Oliphant, G. Cooperstein, S.A. Goldstein, and D. Mosher, Bull. Am. Phys. Soc. *24*, 1031 (1979)

5. J.R. Greig, D.W. Koopman, R.F. Fernsler, R.E. Pechacek, I.M. Vitkovitsky, and A.W. Ali, Phys. Rev. Lett. *41*, 174-177 (1978)

6. D.W. Koopman, J.R. Greig, R.E. Pechacek, A.W. Ali, I.M. Vitkovitsky, and R.F. Fernsler, J. DePhysique Coll. 7. Suppl. 7., Tome 40 p. 419-420 (1979)

7. M. Raleigh, J.R. Greig, and R.E. Pechacek, Bull. Am. Phys. Soc. 24, 978 (1979)

8. M. Raleigh, J.C. Halle, R.E. Pechacek, R.B. Fiorito, E. Laikin, and J.R. Greig, IEEE Conference Record-Abstracts, 1980 IEEE International Conference on Plasma Science, p. 83, (May, 1980)

9. J.R. Greig and R.E. Pechacek, NRL MR 3461 (1977) (unpublished)

10. D.E. Lencioni, "Optical Propagation in the Atmosphere", in NATO AGARD Conference Proceedings No. 138, 32-1 (May, 1976)

11. F. Burhorn & R. Wienecke, Z. Phys. Chem. *215*, 269-284 (1960)

12. Y.B. Zeldovich & Y.P. Raizer, "Physics of Shock Waves and High Temperature Phenomena", Academic Press, New York 1966, Vol I, p. 188

13. E.V. Stupochenko, I.P. Stakhanov, E.V. Samuilov, A.S. Pleshanov, and I.B. Bozhdestvenskii, in "Physical Gas dynamics" Edtd. A.S. Fredvoditelev, Pergamon Press, N.Y. 1961, p. 1-40

14. V.A. Parfenov, L.N. Pakhomov, V.Yu. Petruńkin, and V.A. Podlevski, Sov. Tech. Phys. Lett. 2(8), 286-287 (1977)

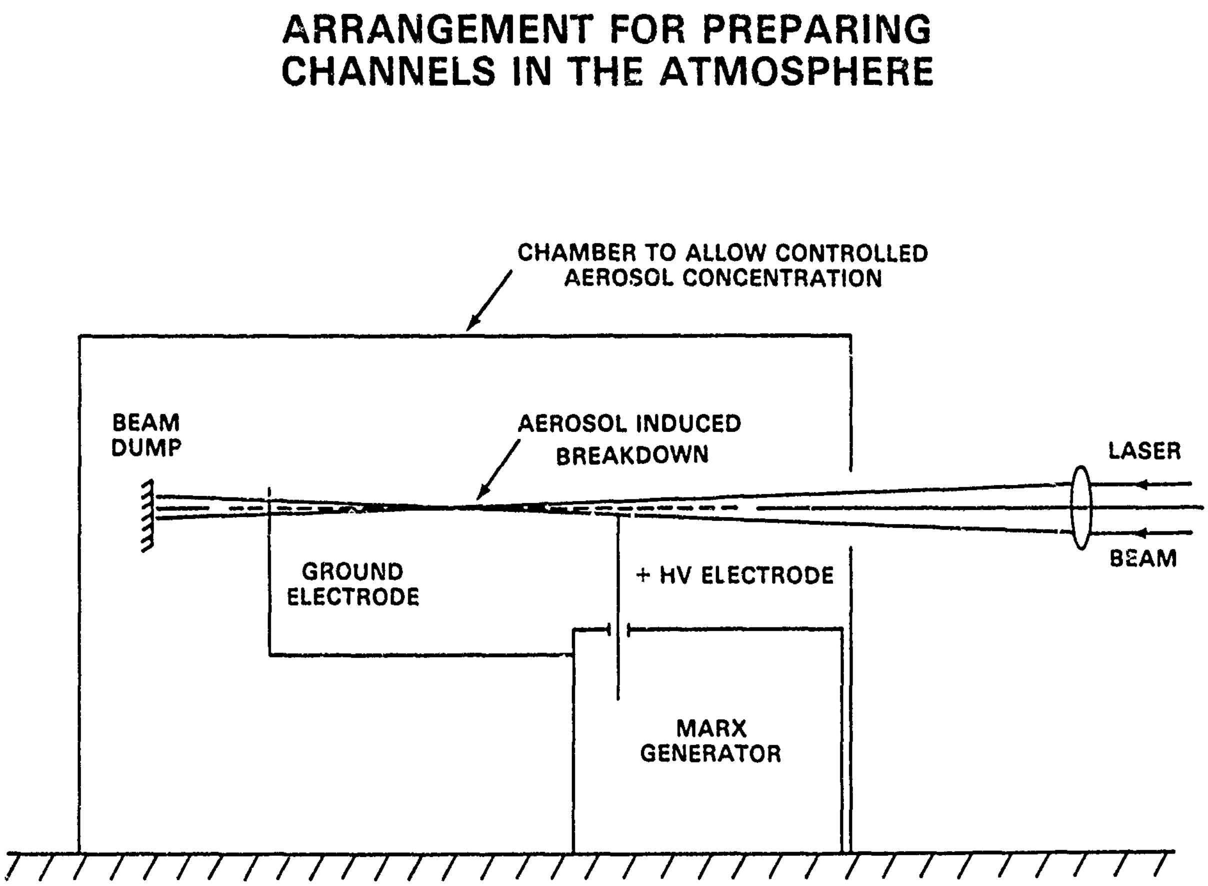

Fig. 1 — The experimental arrangement used to produce the laser-initiated, reduced density channels.

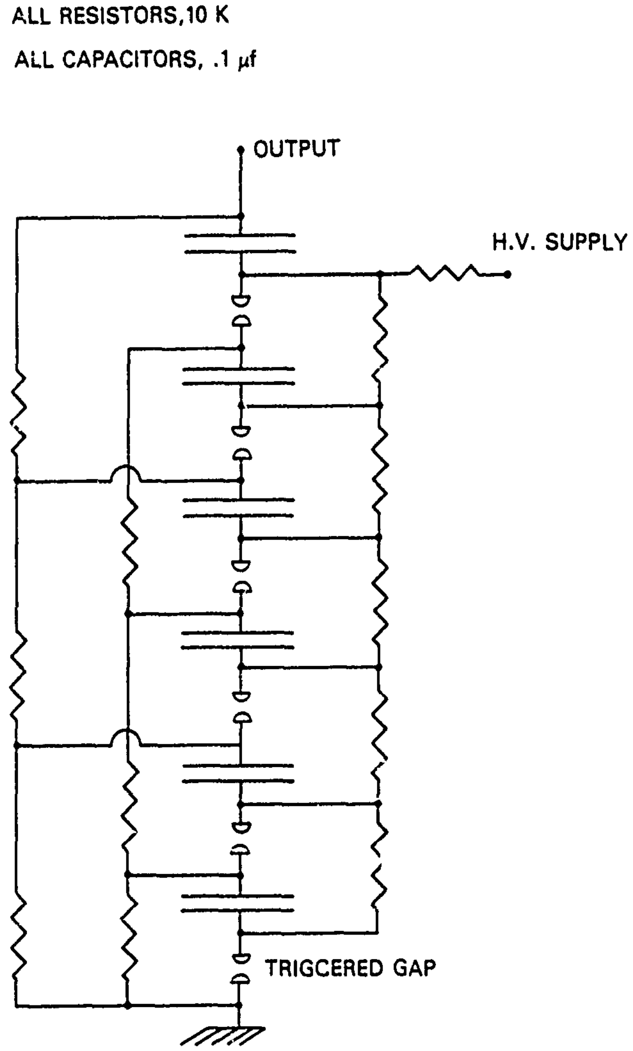

Fig. 2 — The internal connections of the ~360 kV Marx generator.

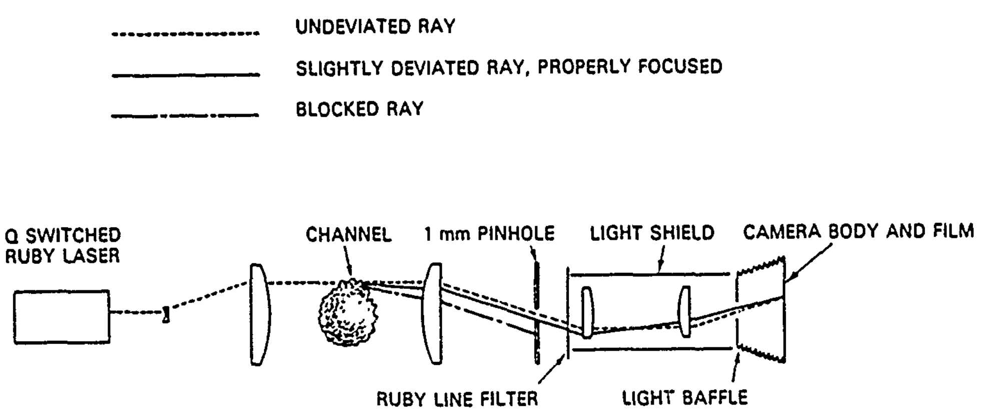

Fig. 3 — The Schlieren system, incorporating object to film plane imaging and image size reduction.

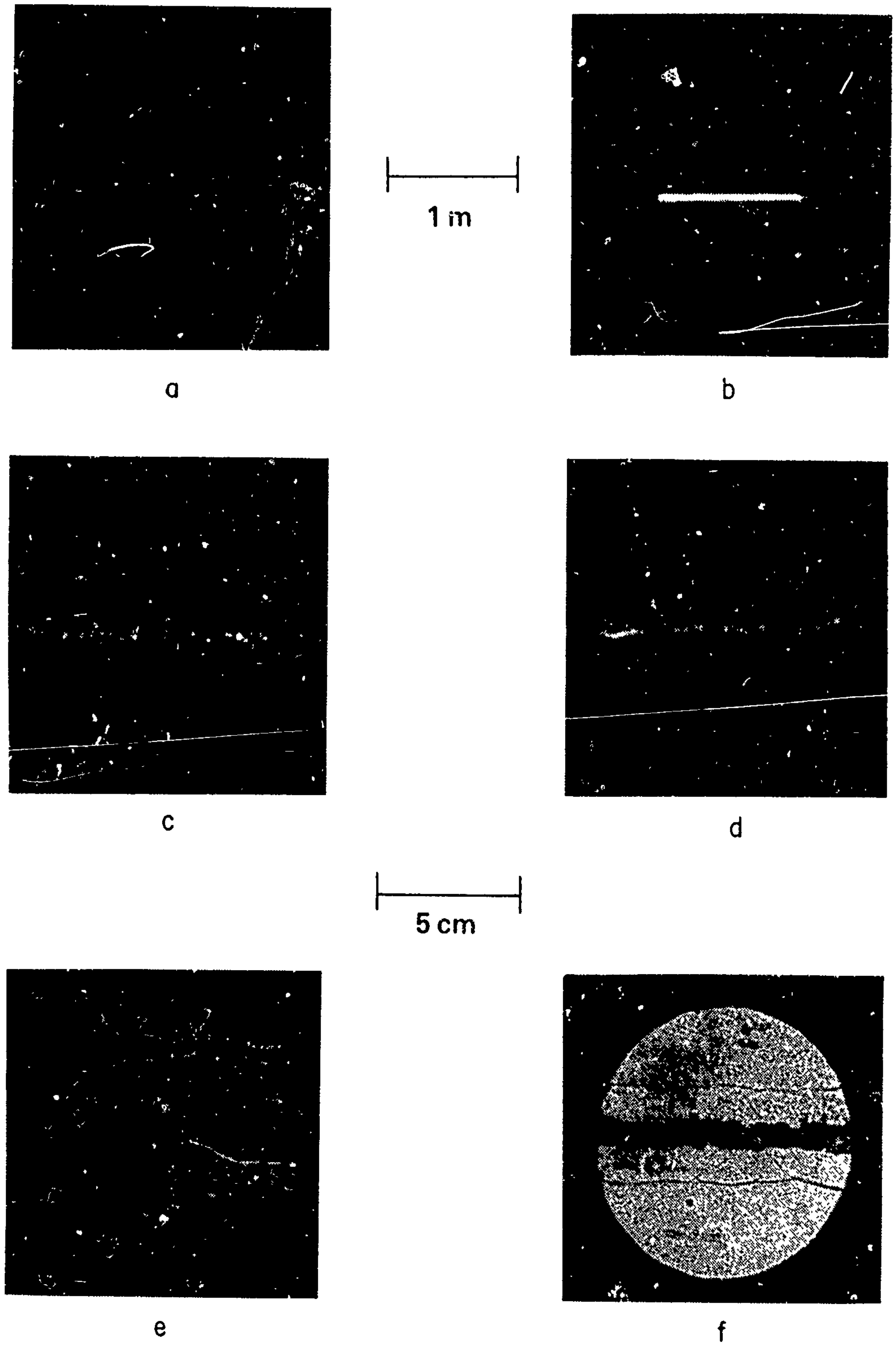

Fig 4 — Open shutter and Schlieren photographs a) Open shutter camera view of an entire string of laser breakdown beads b) Open shutter camera view of a ~ 1 m electric discharge guided by the laser breakdown c) Open shutter camera close-up of the laser breakdown beads d) Open, shutter camera close-up of the guided discharge e) Schlieren photograph of the laser breakdown beads after $\sim 30\ \mu s$ i e just prior to the application of the high voltage discharge f) Schlieren photograph $\sim 1\ \mu s$ after the start of the high voltage discharge, i e, approximately at the first current maximum

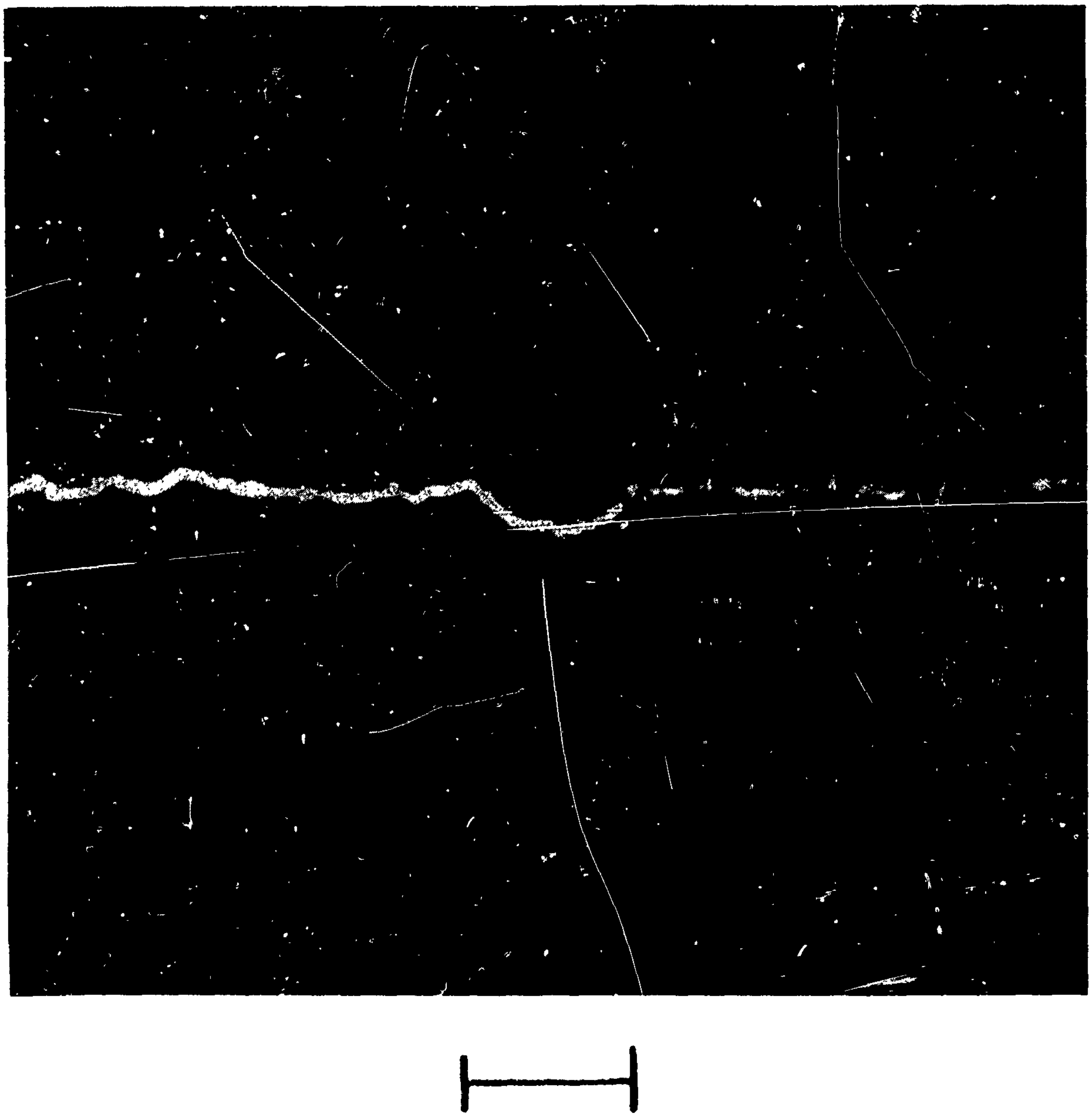

Fig 5 — An open shutter photograph showing a loop in the electric discharge resulting from a gap in the laser breakdown beads

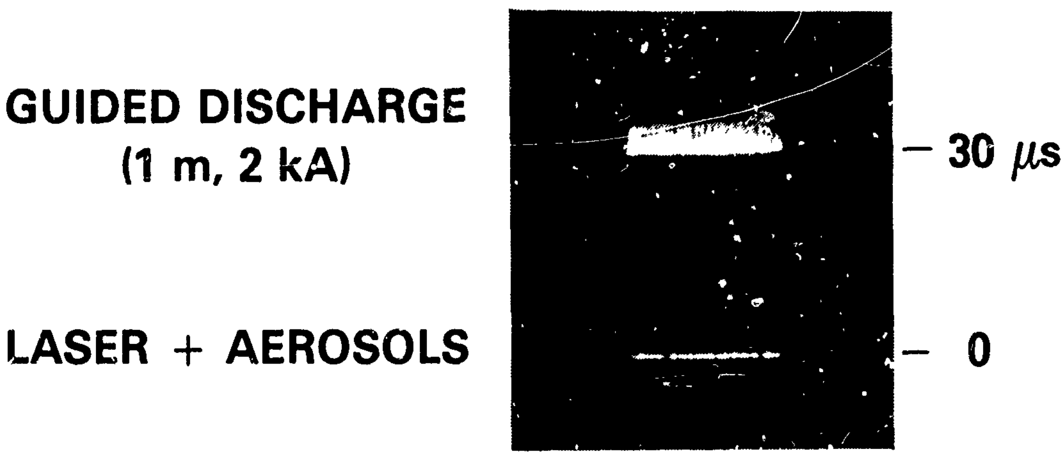

Fig. 6 — A streak photograph showing the laser breakdown and the subsequent guided electric discharge. A ~250 Ω current limiting resistor was used in series with the Marx generator to give comparable exposures for the laser breakdown and the discharge.

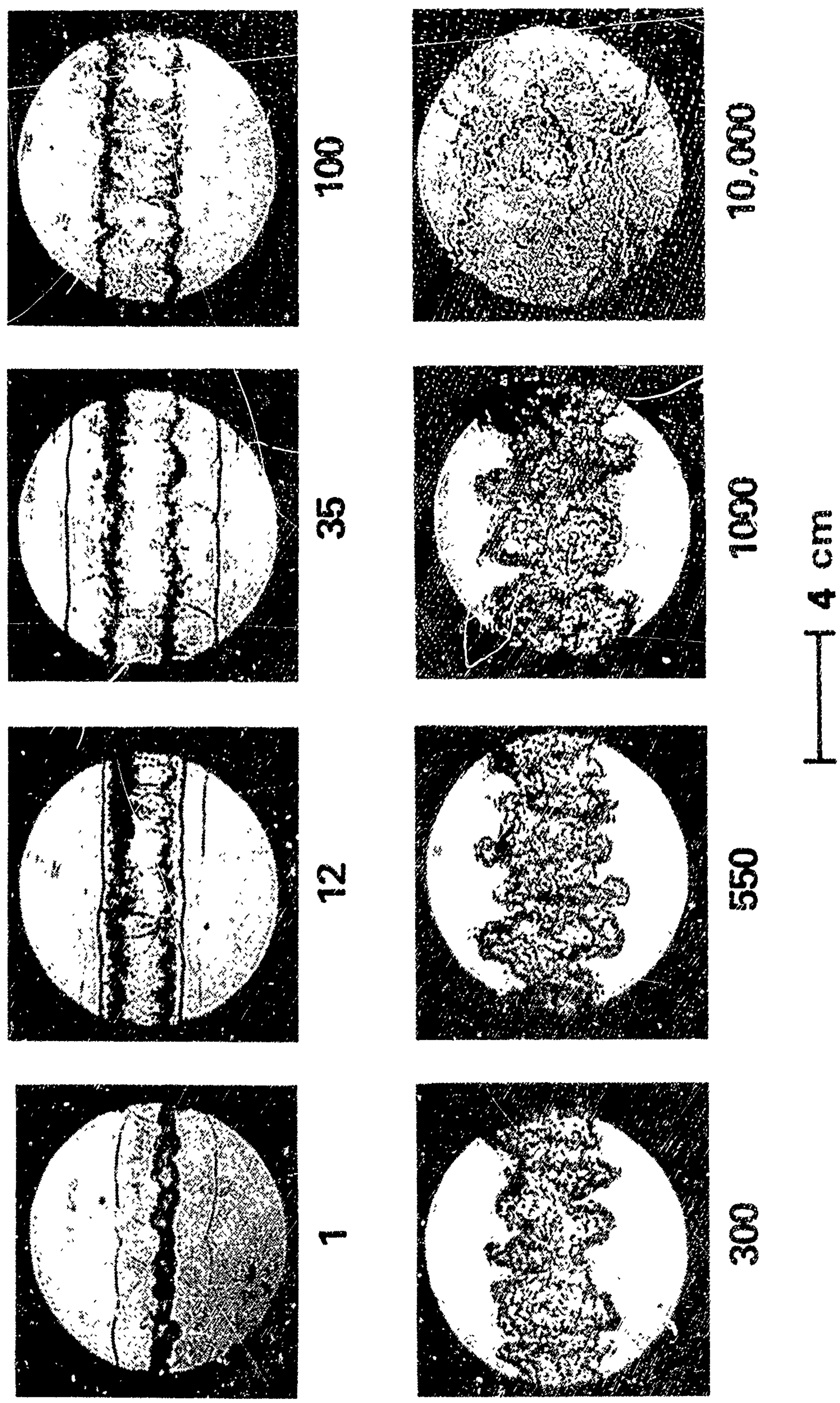

Fig. 7 — A series of Schlieren photographs showing the time history of the channel. The delay between the start of the electric discharge and the time of the photograph is quoted in μs beneath each picture.

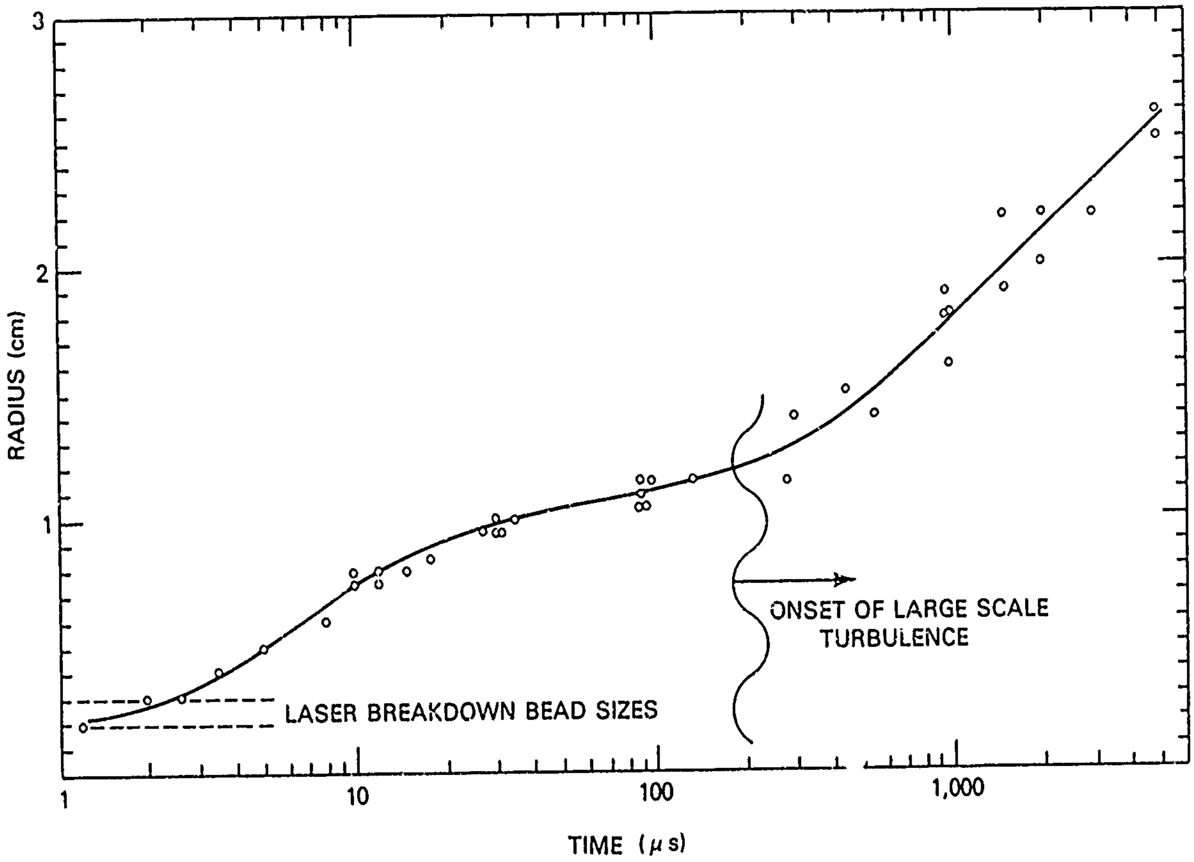

Fig. 8 — The average channel radius as a function of time as determined by Schlieren photography. The points represent individual shots.

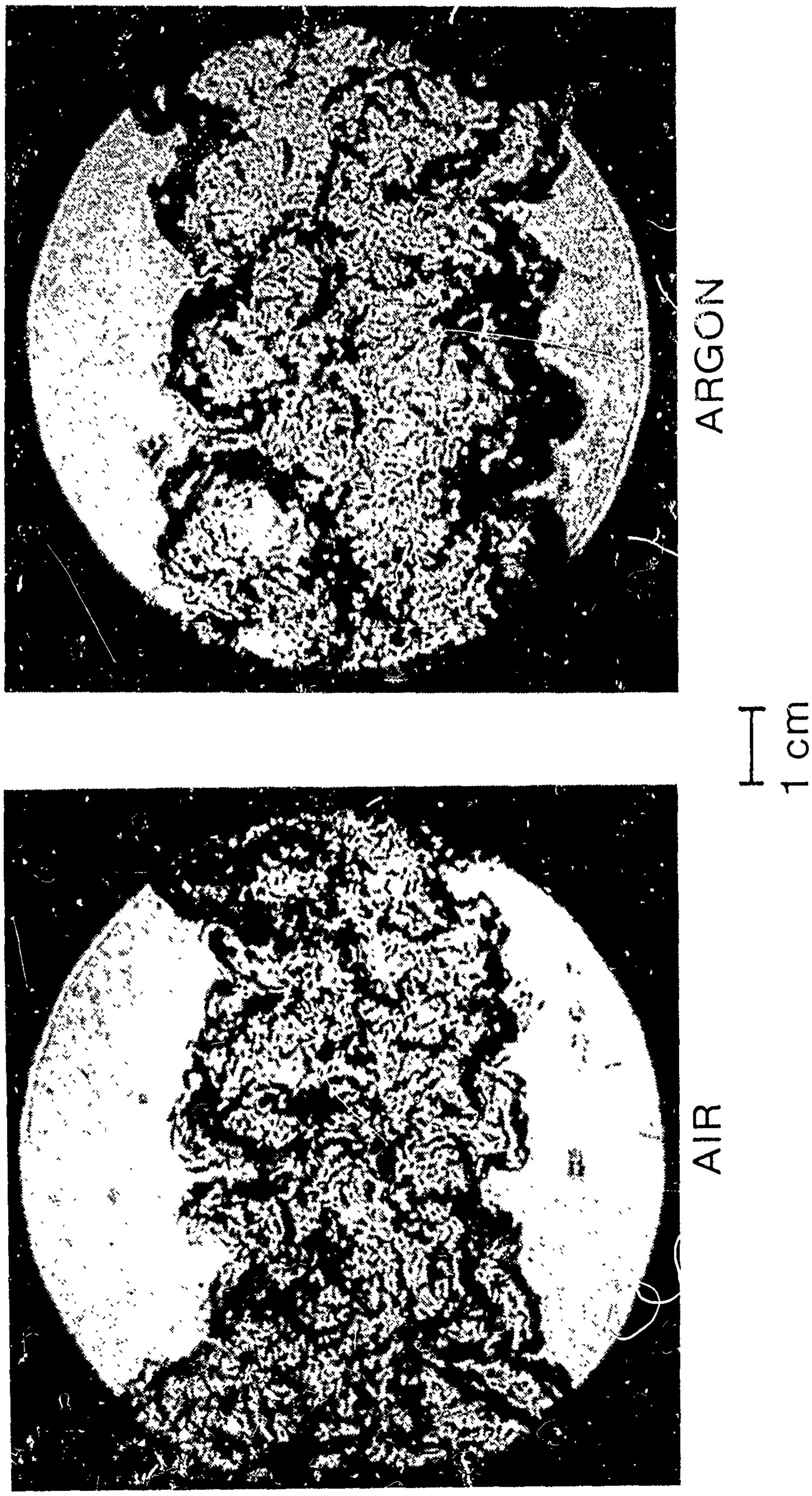

Fig. 9 – Schlieren photographs of channels in air and Argon 960 μs after the electric discharge.

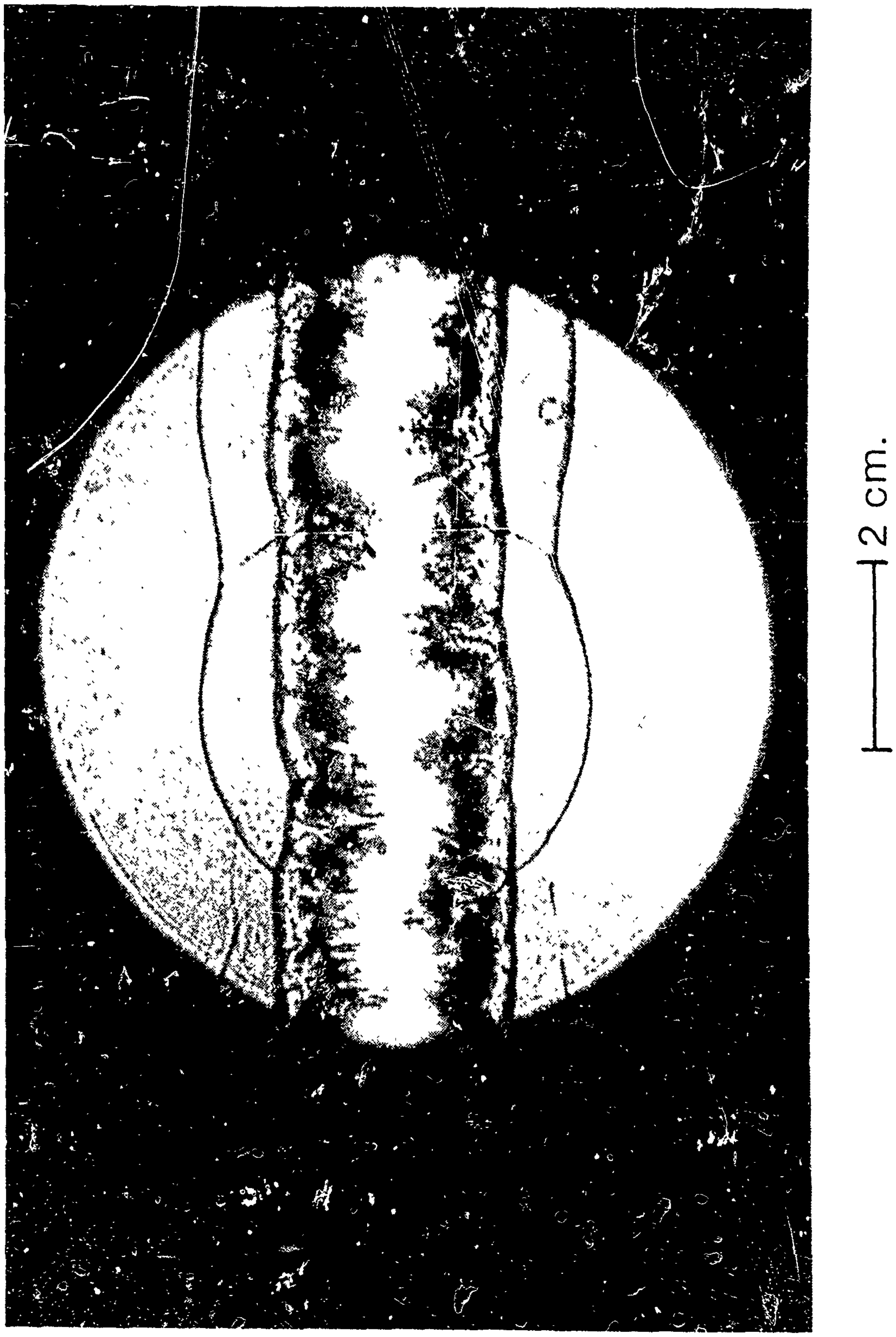

Fig 10 — A superimposed self light and Schlieren image of one shot The photograph was produced by removing the ruby line filter from the Schlieren System The ruby laser fired $\sim 12\ \mu s$ after the start of the electric discharge

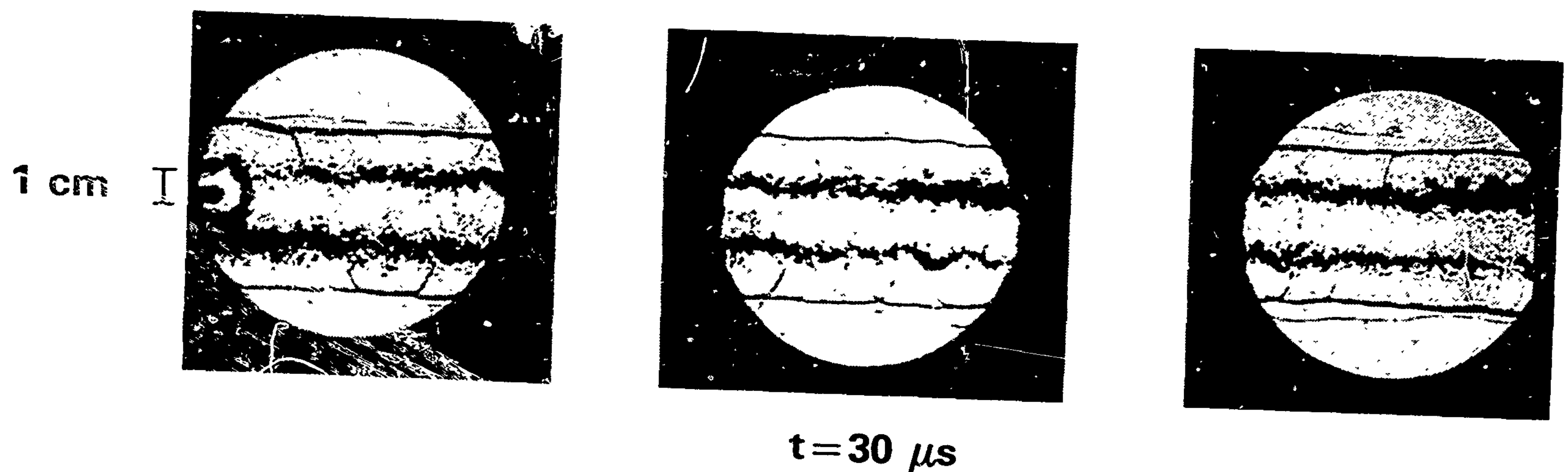

Fig. 11 — Schlieren photographs taken at the high voltage electrode, near mid channel, and at the ground electrode for a 1 m long guided discharge. All photographs were taken ~30 μs after the start of the electric discharge.

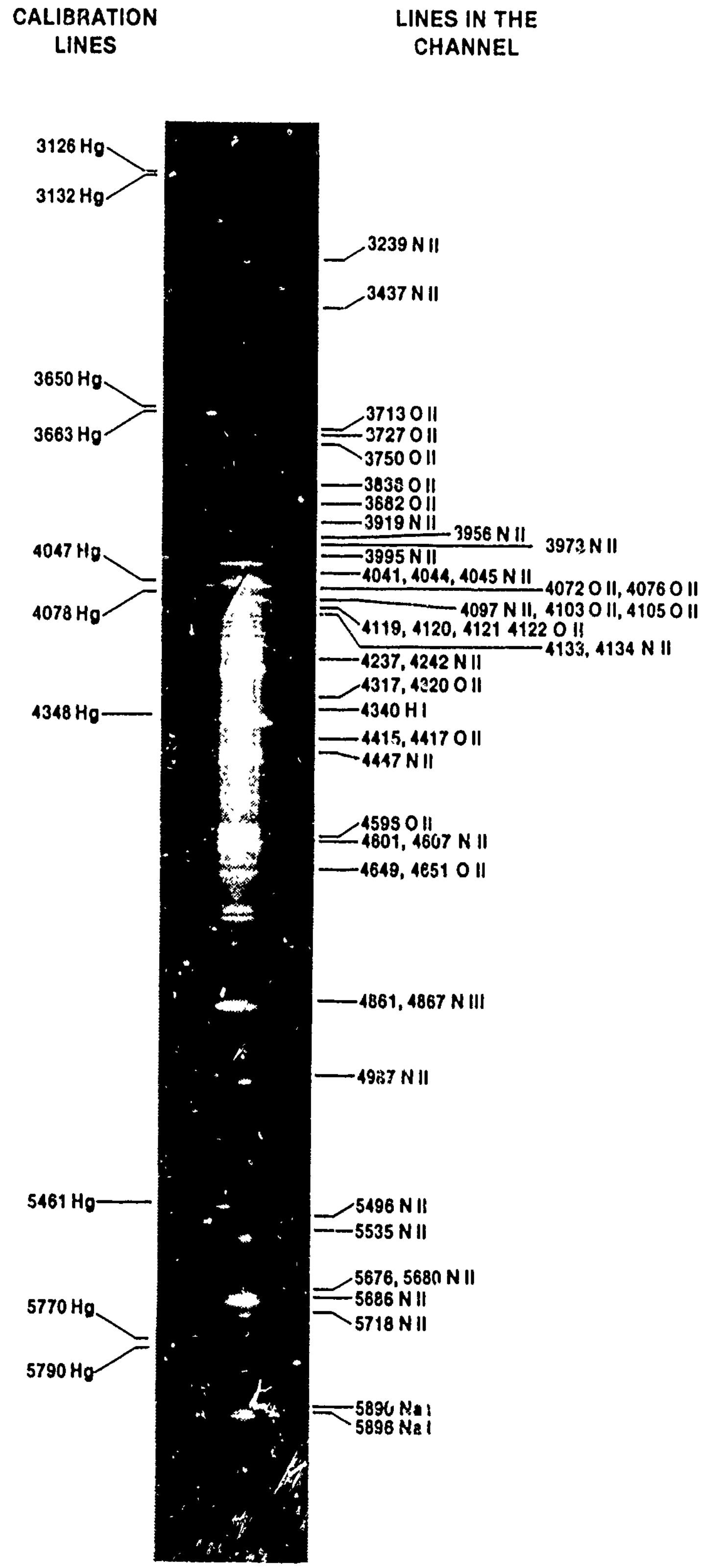

Fig. 12 — The time integrated visible spectrum of the channel. The spectrum is dominated by NII and OII lines

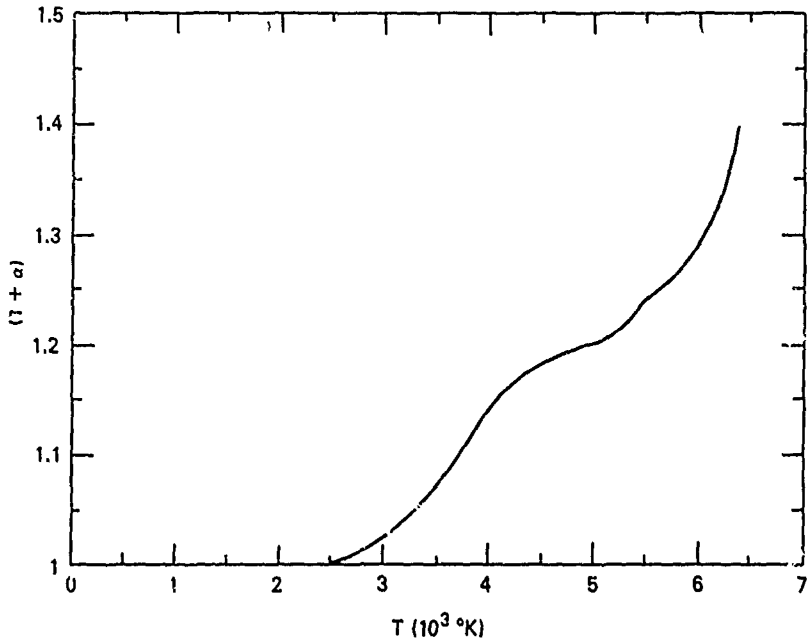

Fig. 13 — The dissociation of atmospheric pressure air as a function of temperature, as computed from the tables of Burhorn and Wienecke.[11]

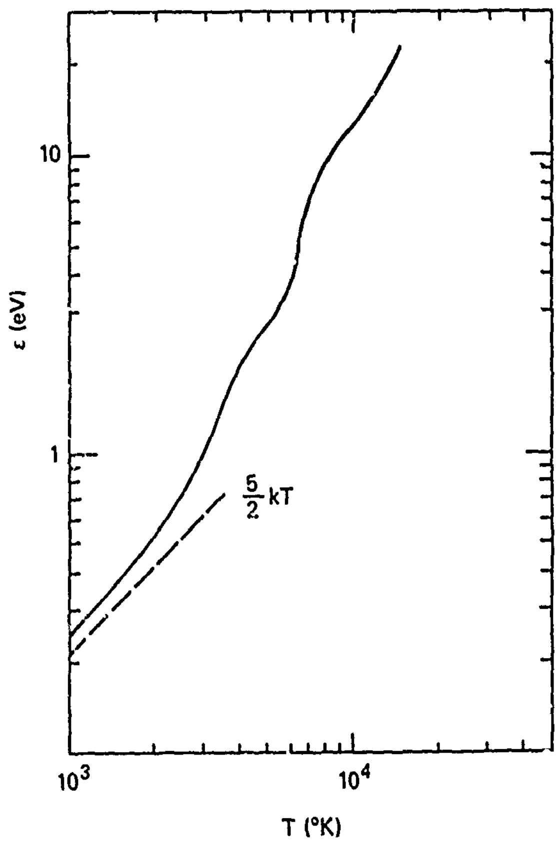

Fig. 14 — The total interna energy (kinetic + rotational + vibrational + dissociation) per original molecule, for air at atmospheric pressure, as computed from the tables of Burhorn and Wienecke.[11]

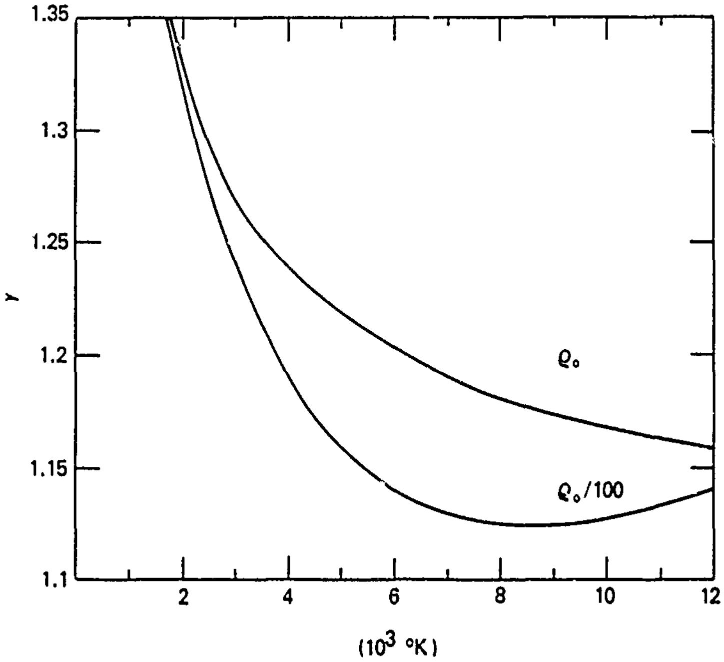

Fig. 15 — The effective adiabatic exponent, γ, for normal and reduced density air, as a function of temperature, as given in the tables of Zel'dovich and Raizer.[12]

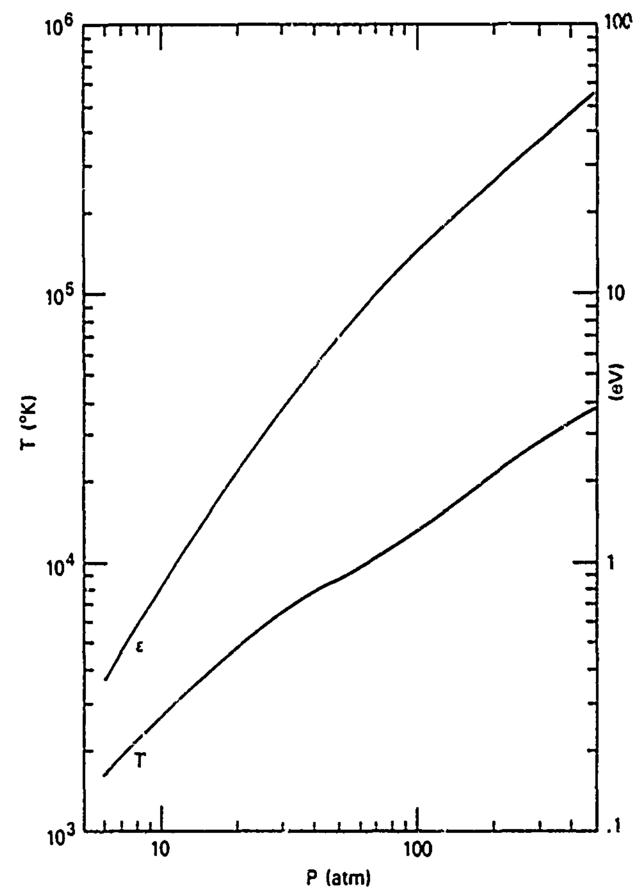

Fig. 16 — The temperature and total internal energy of normal density air as functions of pressure, as given in the tables of Zel'dovich and Raizer.[12]

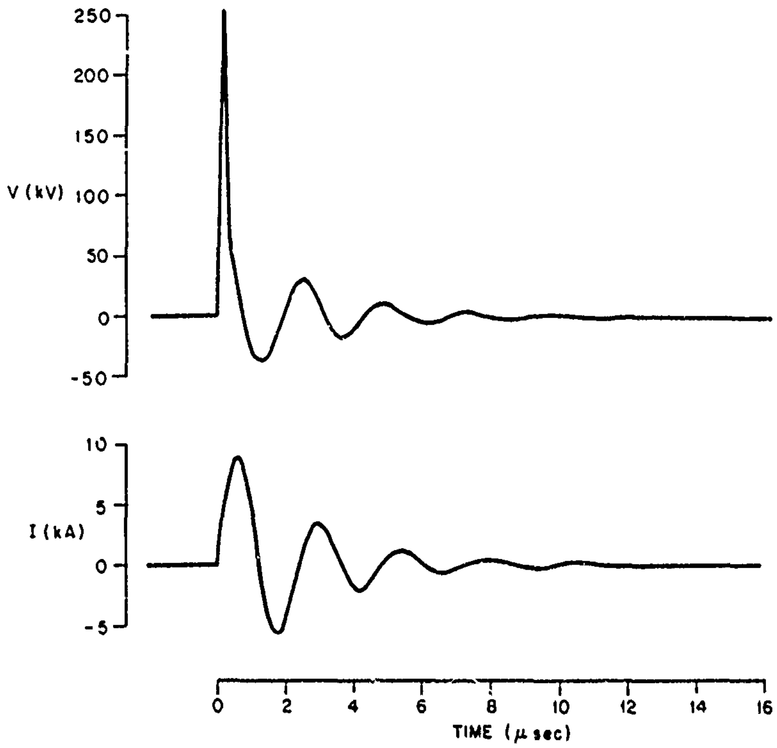

Fig. 17 — The voltage and current for a .5 m guided electric discharge.

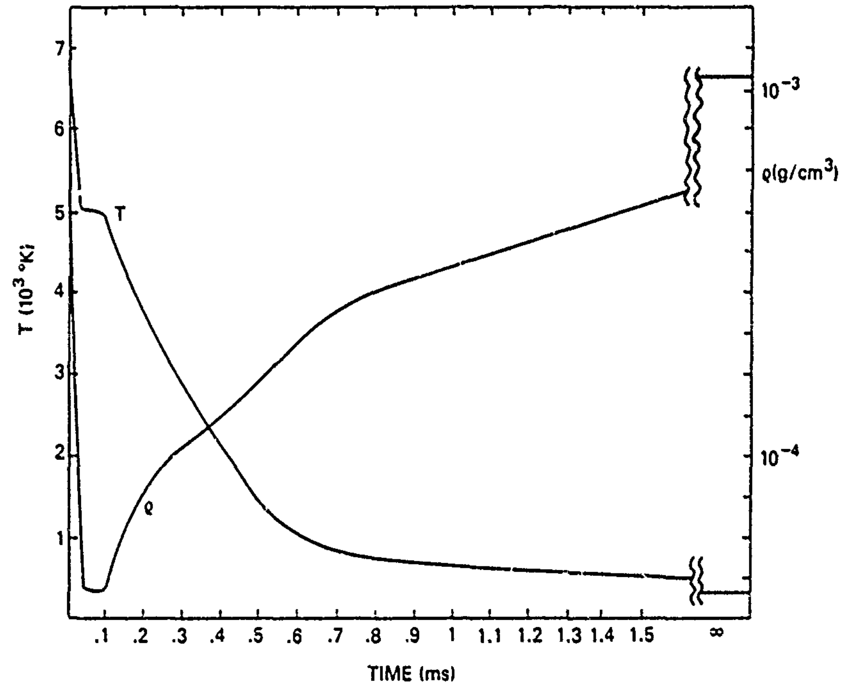

Fig. 18 — The temperature and density of the channel as functions of time. These results are computed by the methods discussed in section III.

DISTRIBUTION LIST

1. Commander
   Naval Sea Systems Command
   Department of the Navy
   Washington, D.C. 20363
   ATTN: NAVSEA 03H (Dr. C.F. Sharn)

2. Central Intelligence Agency
   P.O. Box 1925
   Washington, D.C. 20013
   ATTN: Dr. C. Miller/OSI

3. Air Force Weapons Laboratory
   Kirtland Air Force Base
   Albuquerque, New Mexico 87117
   ATTN: Lt. Col. J.H. Havey

4. U.S. Army Ballistics Research Laboratory
   Aberdeen Proving Ground, Maryland 21005
   ATTN: Dr. D. Eccleshall (DRXBR-BM)

5. Ballistic Missile Defense Advanced Technology Center
   P.O. Box 1500
   Huntsville, Alabama 35807
   ATTN: Dr. L. Harvard (BMDSATC-1)

6. B-K Dynamics Inc.
   15825 Shady Grove Road
   Rockvile, Maryland 20850
   ATTN: Mr. I. Kuhn

7. Intelcom Rad Tech
   P.O. Box 81087
   San Diego, California 92183
   ATTN: Mr. W. Selph

8. Lawrence Livermore Laboratory
   University of California
   Livermore, California 94550
   ATTN: Dr. R.J. Briggs
   Dr. T. Fessenden
   Dr. E.P. Lee

9. Mission Research Corporation
   735 State Street
   Santa Barbara, California 93102
   ATTN: Dr. C. Longmire
   Dr. N. Carron

10. National Bureau of Standards
    Gaithersburg, Maryland 20760
    ATTN: Dr. Mark Wilson

11. Science Applications, Inc.
1200 Prospect Street
LaJolla, California 92037
ATTN: Dr. M.P. Fricke
Dr. W.A. Woolson

12. Science Applications, Inc.
Security Office
5 Palo Alto Square, Suite 200
Palo Alto, California 94304
ATTN: Dr. R.R. Johnston
Dr. Leon Feinstein

13. Science Applications, Inc.
1651 Old Meadow Road
McLean, Virginia 22101
ATTN: Mr. W. Chadsey

14. Science Applications, Inc.
8201 Capwell Drive
Oakland, California 94621
ATTN: Dr. J.E. Reaugh

15. Naval Surface Weapons Center
White Oak Laboratory
Silver Spring, Maryland 20910
ATTN: Mr. R.J. Biegalski
Dr. R. Cawley
Dr. J.W. Forbes
Dr. D.L. Love
Dr. C.M. Huddleston
Mr. W.M. Hinckley
Dr. G.E. Hudson
Mr. G.J. Peters
Mr. N.E. Scofield
Dr. E.C. Whitman
Dr. M.H. Cha
Dr. H.S. Uhm
Dr. R.B. Fiorito

16. C.S. Draper Laboratories
Cambridge, Massachusetts 02139
ATTN: Dr. E. Olsson
Dr. L. Matson

17. M.I.T. Lincoln Laboratories
P.O. Box 73
Lexington, Massachusetts 02173
ATTN: Dr. J. Salah

18. Physical Dynamics, Inc.
P.O. Box 1883
LaJolla, California 92038
ATTN: Dr. K. Brueckner

19. Office of Naval Research
Department of the Navy
Arlington, Virginia 22217
ATTN: Dr. W.J. Condell (Code 421)

20. Avco Everett Research Laboratory
2385 Revere Beach Pkwy.
Everett, Massachusetts 02149
ATTN: Dr. R. Patrick
Dr. Dennis Reilly

22. Naval Research Laboratory
Washington, D.C. 20375
ATTN: M. Lampe — Code 4792
M. Friedman — Code 4700.1
J.R. Greig — Code 4763 (50 copies)
I.M. Vitkovitsky — Code 4770
T. Coffey — Code 4000
Superintendent, Plasma Physics Div. — Code 4700 (25 copies)
Library — Code 2628 (20 copies)
A. Ali — Code 4700.1T
D. Book — Code 4040
J. Boris — Code 4040
S. Kainer — Code 4790
A. Robson — Code 4760
M. Picone — Code 4040
D. Spicer — Code 4169
M. Raleigh — Code 4763
R. Pechacek — Code 4763
J.D. Sethian — Code 4762
K.A. Gerber — Code 4762
D.N. Spector — Code 4762

23. Defense Advanced Research Projects Agency
1400 Wilson Blvd.
Arlington, Virginia 22209
ATTN: Dr. J. Mangano
Dr. J. Bayless

24. JAYCOR
205 S. Whiting St.
Alexandria, Virginia 22304
ATTN: Drs. D. Tidman
R. Hubbard
J. Gillory

25. JAYCOR
Naval Research Laboratory
Washington, D.C. 20375
ATTN: Dr. R. Fernsler — 4770
Dr. G. Joyce — Code 4790
Dr. S. Goldstein — Code 4770

26. SAI
Naval Research Laboratory
Washington, D.C. 20375
ATTN: A. Drobot — Code 4790
W. Sharp — Code 4790

27. Physics International, Inc.
2700 Merced Street
San Leandro, CA
ATTN: Dr. J. Maenchen
Dr. E. Goldman

28. Mission Research Corp.
1400 San Mateo, S.E.
Albuquerque, NM 87108
ATTN: Dr. Brendan Godfrey

29. Princeton University
Plasma Physics Laboratory
Princeton, NJ 08540
ATTN: Dr. F. Perkins, Jr.

30. McDonnell Douglas Research Laboratories
Dept. 223, Bldg. 33, Level 45
Box 516
St. Louis, MO 63166
ATTN: Dr. Michael Greenspan

31. Cornell University
Ithaca, NY 14853
ATTN: Prof. David Hammer

32. Sandia Laboratories
Albuquerque, NM 87185
ATTN: Dr. Bruce Miller
Dr. Barbara Epstein
Dr. John Olsen
Dr. Don Cook

33. University of California
Physics Department
Irvine, CA 92717
ATTN: Dr. Gregory Benford

34. Naval Air Systems Command
Washington, D.C. 20361
ATTN: Dr. R.J. Wasneski, Code AIR-350F

35. Beers Associates, Inc.
P.O. Box 2549
Reston, VA 22090
ATTN: Dr. Douglas Strickland

36. U.S. Department of Energy
Washington, D.C. 20545
Office of Fusion Energy ATTN: Dr. W. F. Dove
Office of Inertial Fusion, ATTN: Dr. T. Godlove

37. AFOSR/NP
Bolling Air Force Base
Washington, D.C. 20331
ATTN: Capt. R.L. Gullickson

AD-A095725

ERRATUM

NRL MEMORANDUM REPORT 4380

SPECTRUM OF THE CHANNEL

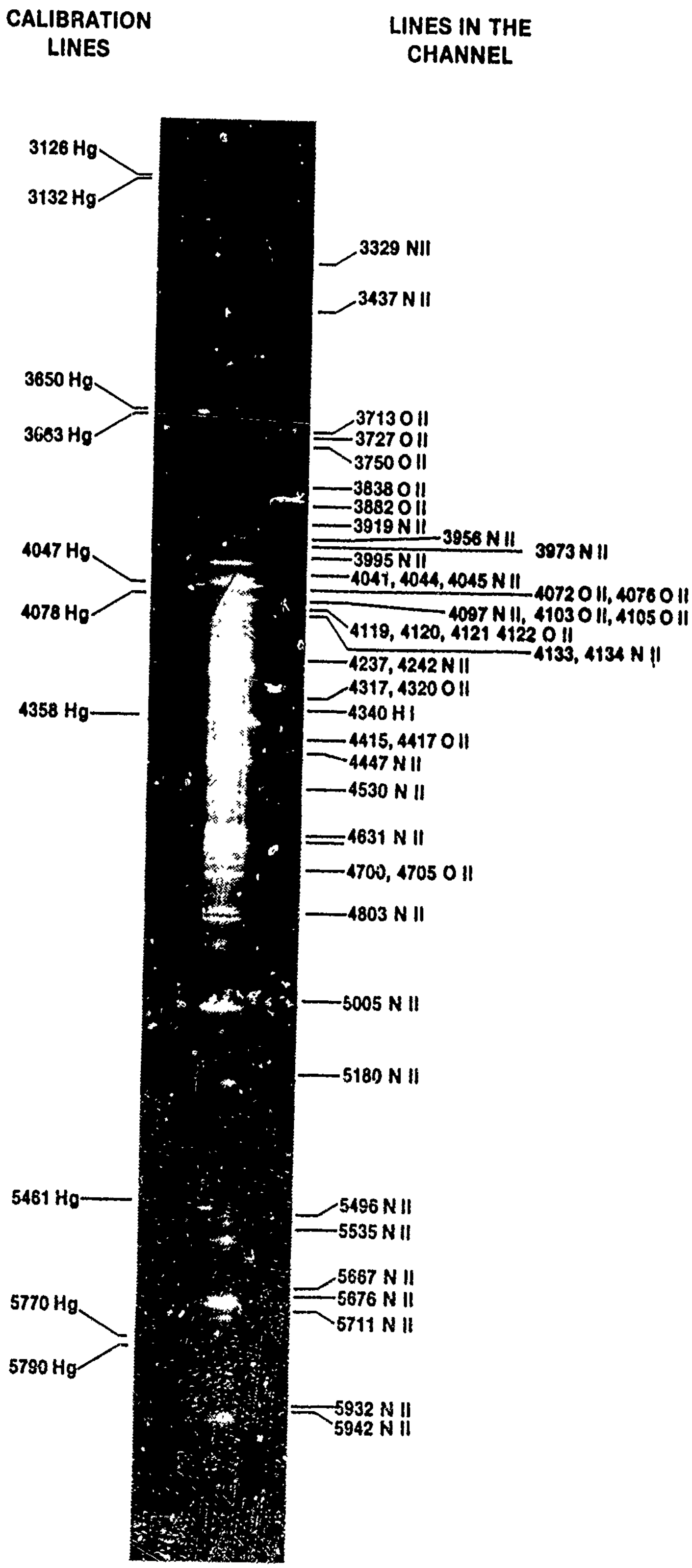

Fig. 12 — The time integrated visible spectrum of the channel. The spectrum is dominated by NII and OII lines.

ERRATUM
NRL MEMORANDUM REPORT 4380

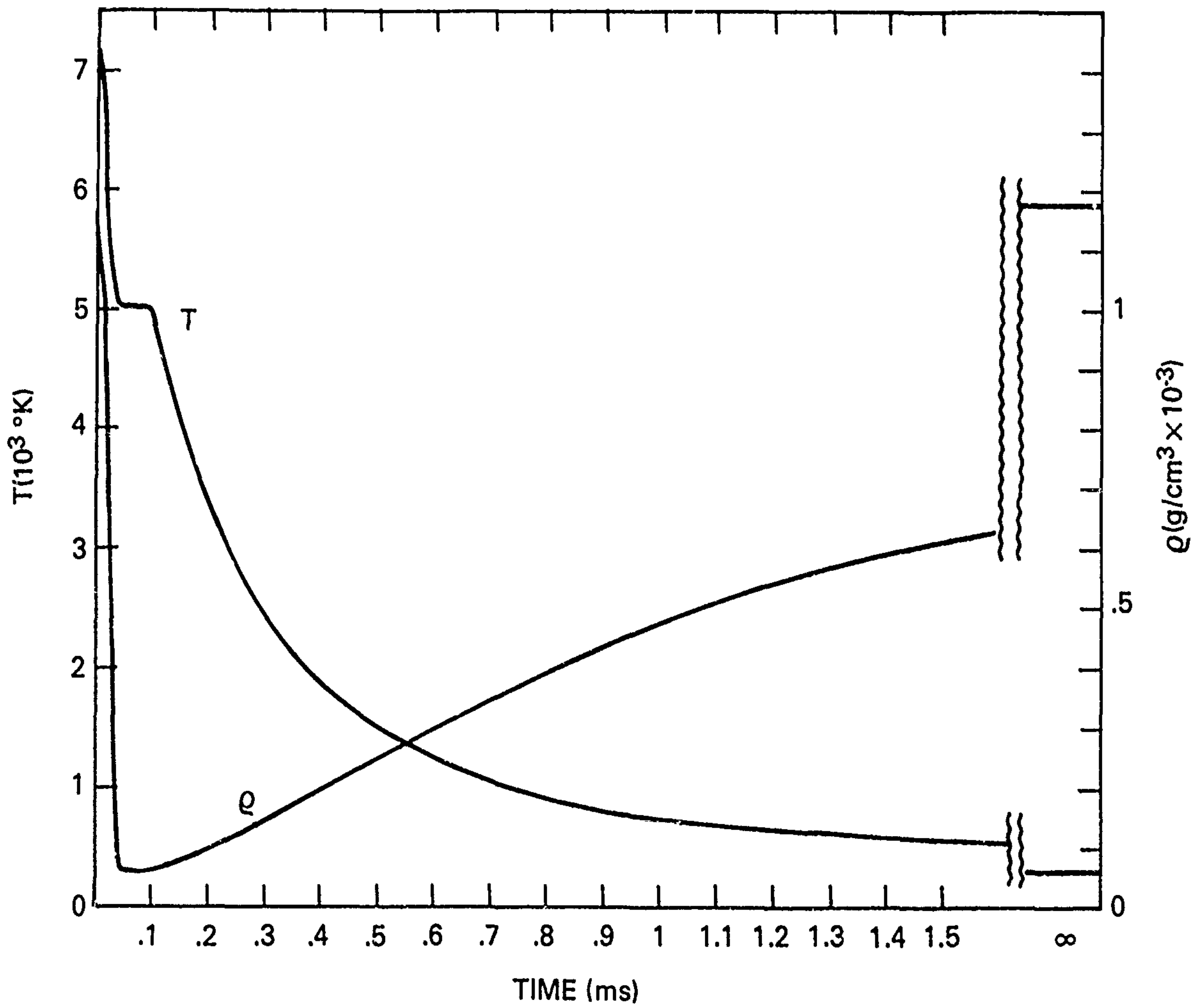

Fig. 18 — The temperature and density of the channel as functions of time. These results are computed by the methods discussed in section III.